REPLACEMENT SHEET

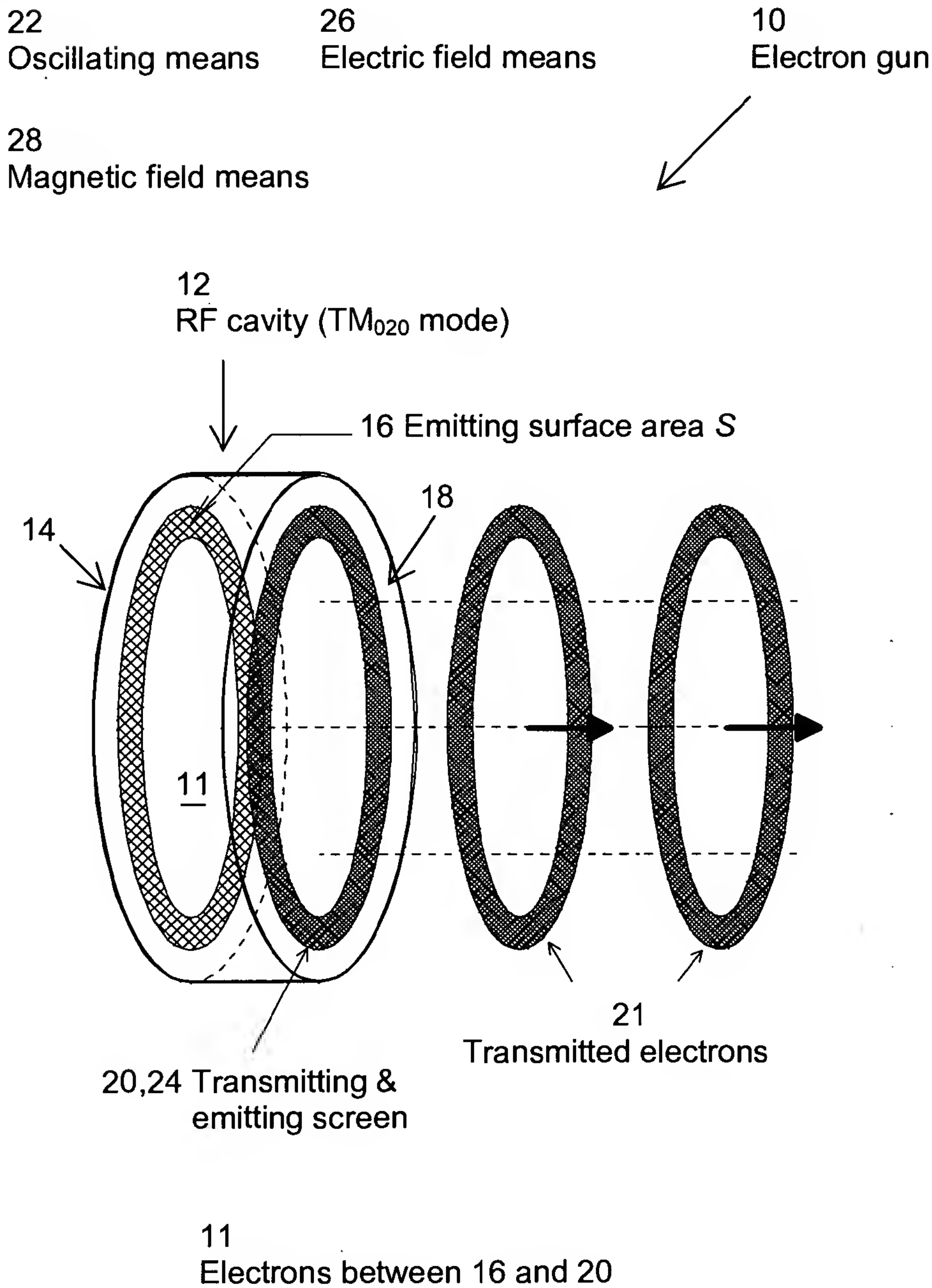

Figure 1: Perspective view of the micropulse gun for a hollow beam in the TM_{020} mode. The inner conductor is not shown.

REPLACEMENT SHEET

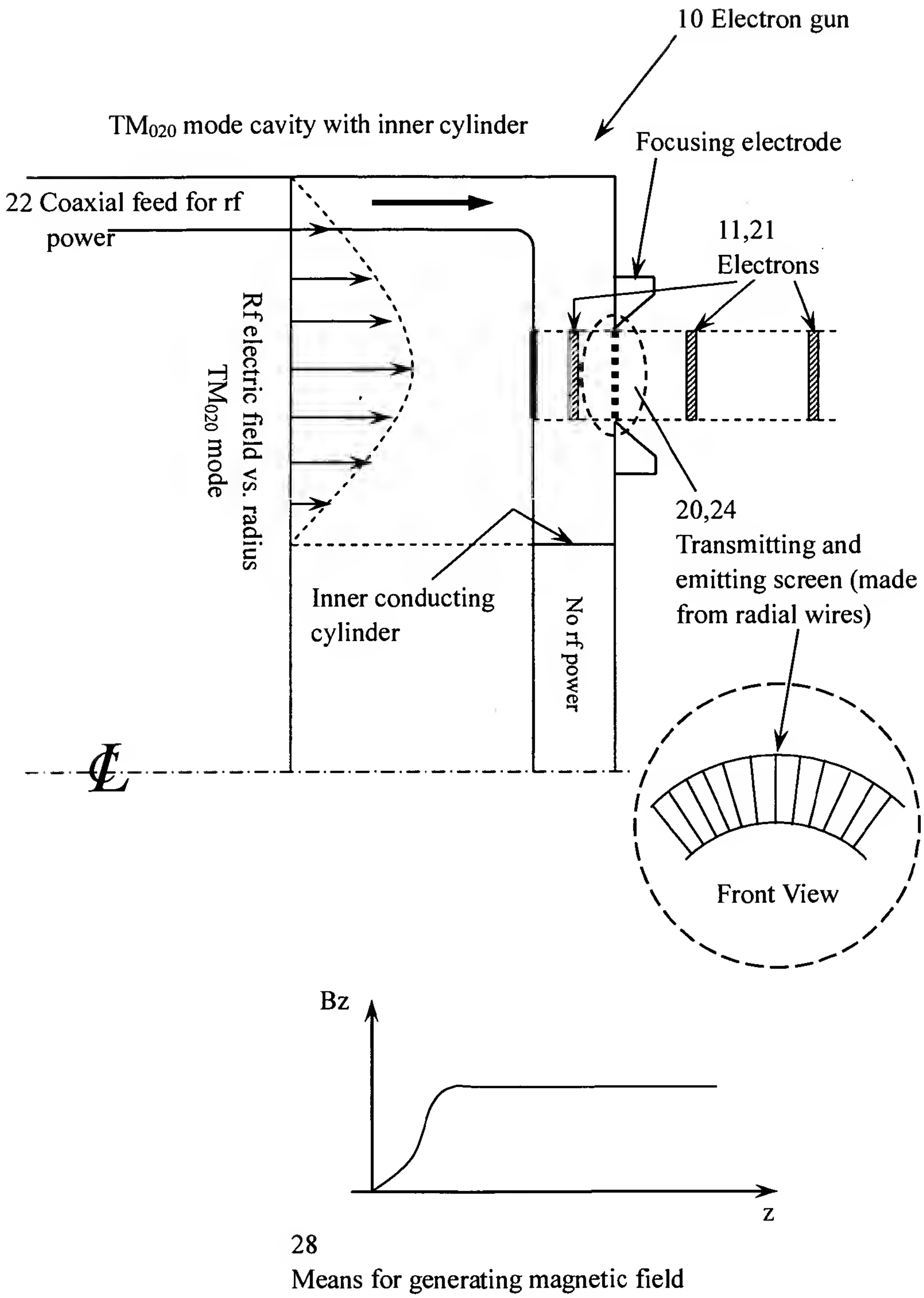

Figure 2: Schematic of rf gun operating in TM_{020} mode.

REPLACEMENT SHEET

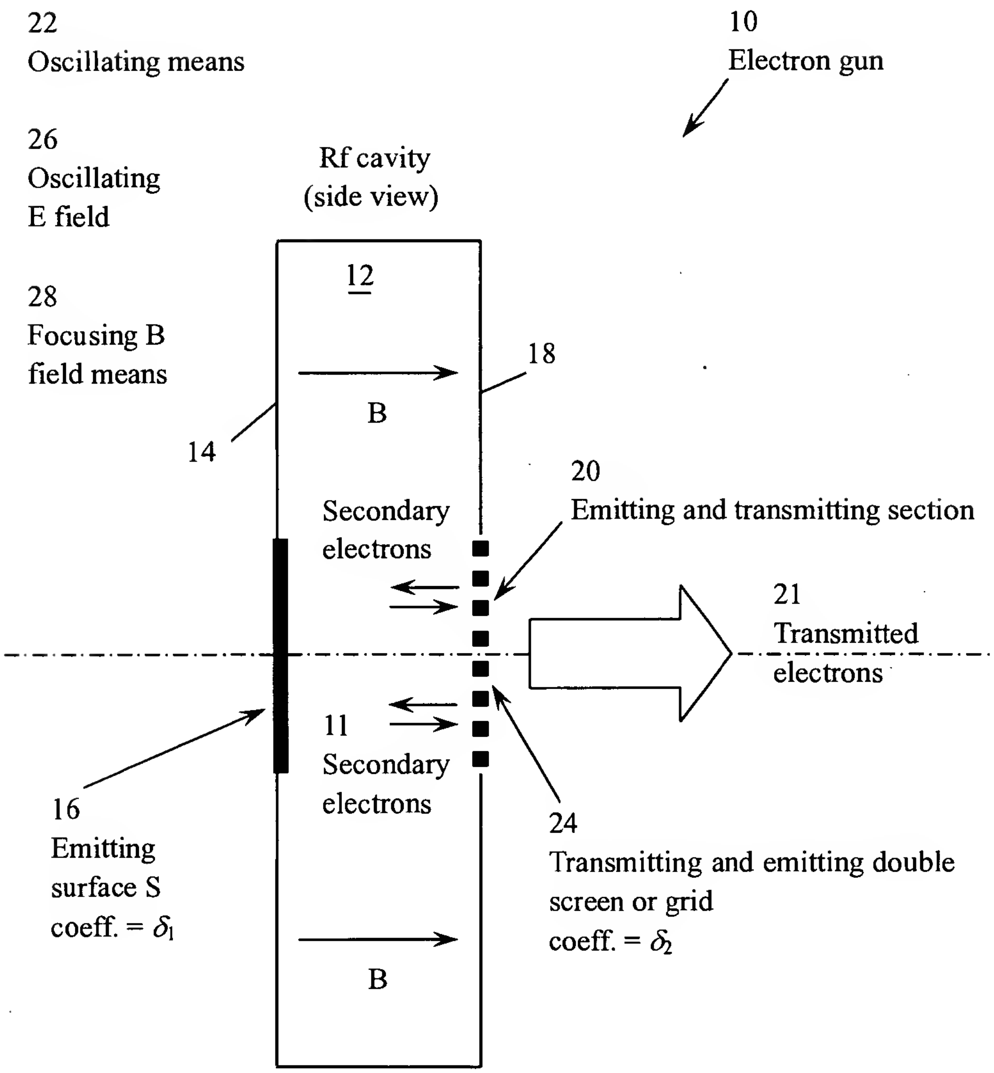

Figure 3: Schematic of micropulse gun for solid beam (TM_{010}) mode. A coaxial feed is used for rf input (not shown).

REPLACEMENT SHEET

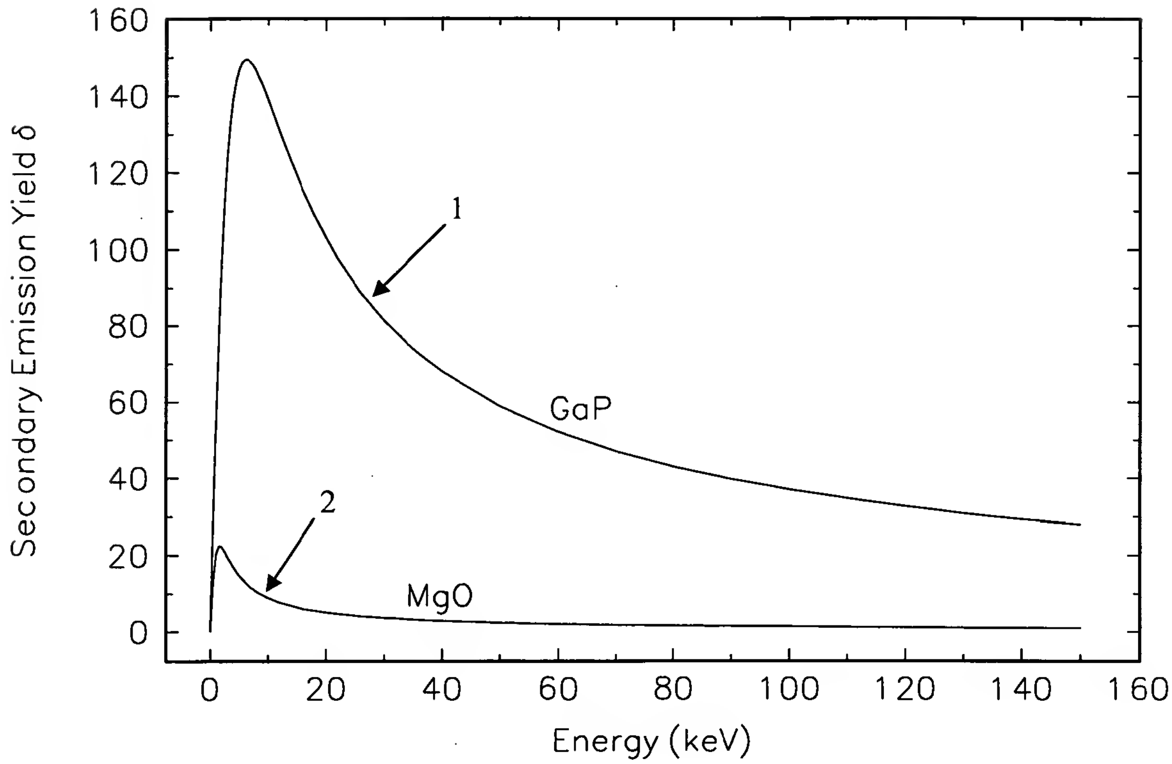

1 – Secondary emission yield of GaP
2 – Secondary emission yield of MgO

Figure 4: Secondary electron emission yield curve for GaP and MgO.

REPLACEMENT SHEET

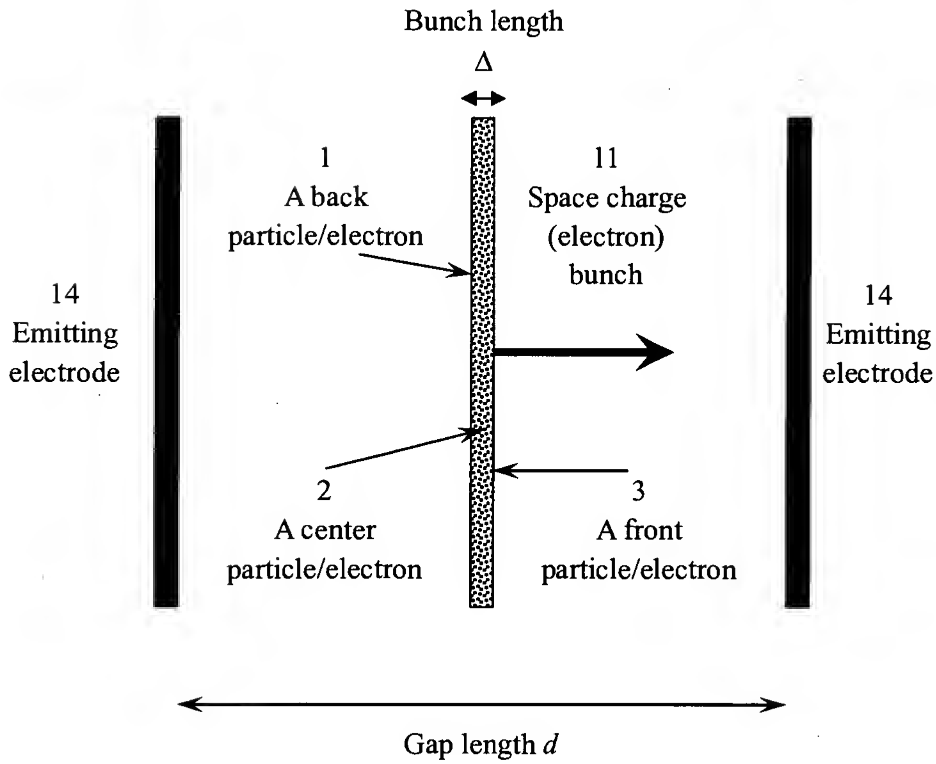

14 - Emitting electrodes
11 - Electron bunch
1 - A back particle/electron
2 - A center particle/electron
3 - A front particle/electron

Figure 5. Schematic drawing of model used in theoretical analysis.

REPLACEMENT SHEET

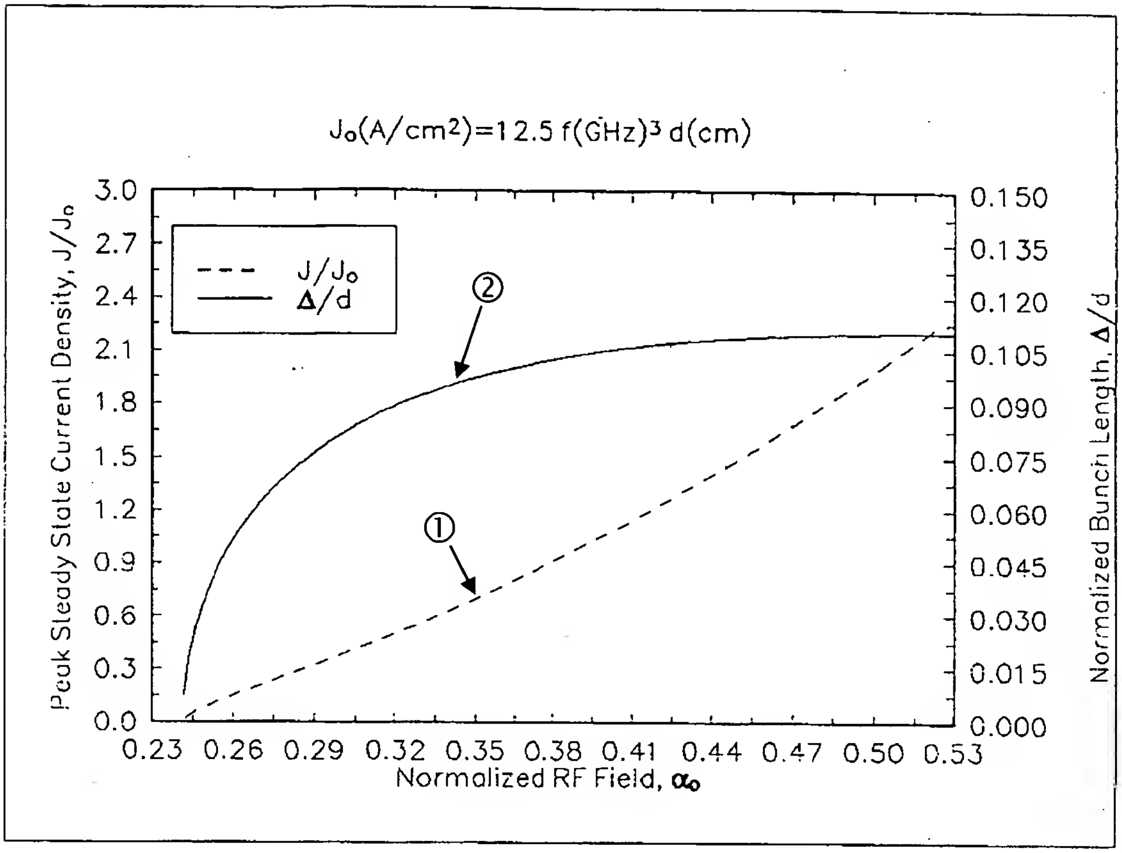

① Plot of normalized peak current density at steady state versus rf field.

② Plot of normalized electron bunch length versus rf field.

Figure 6: Steady-state current density and bunch length vs. rf field, all parameters are normalized.

REPLACEMENT SHEET

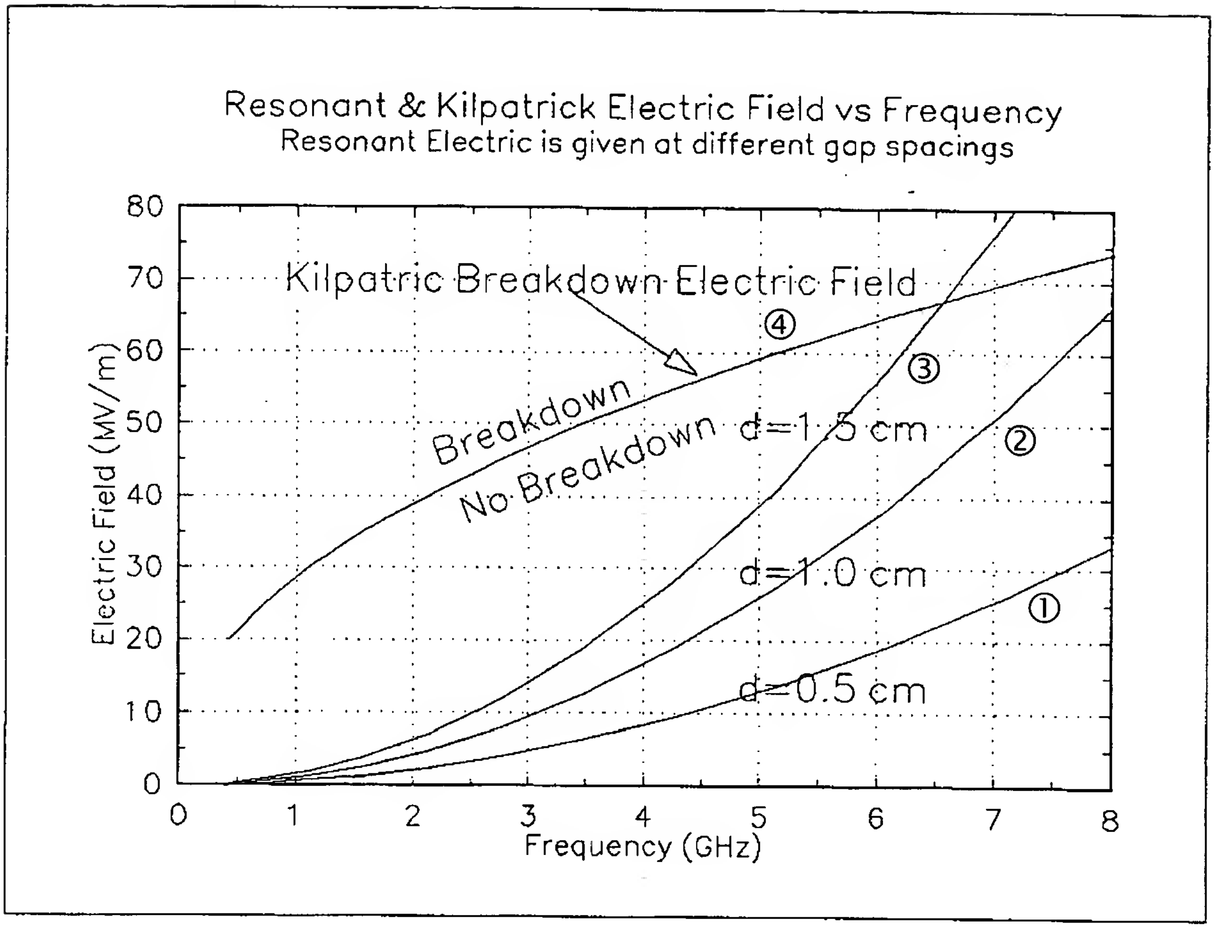

① Plot of resonant electric field versus frequency for 0.5 cm gap

② Plot of resonant electric field versus frequency for 1.0 cm gap

③ Plot of resonant electric field versus frequency for 1.5 cm gap

④ Plot of Kilpatrick breakdown electric field versus frequency.

Figure 7: Plot of resonant electric fields for $\alpha_0 = 0.453$ and various gap spacings. Also shown is the critical Kilpatrick electric field as a function of rf frequency.

REPLACEMENT SHEET

1.3 GHz, xy plot

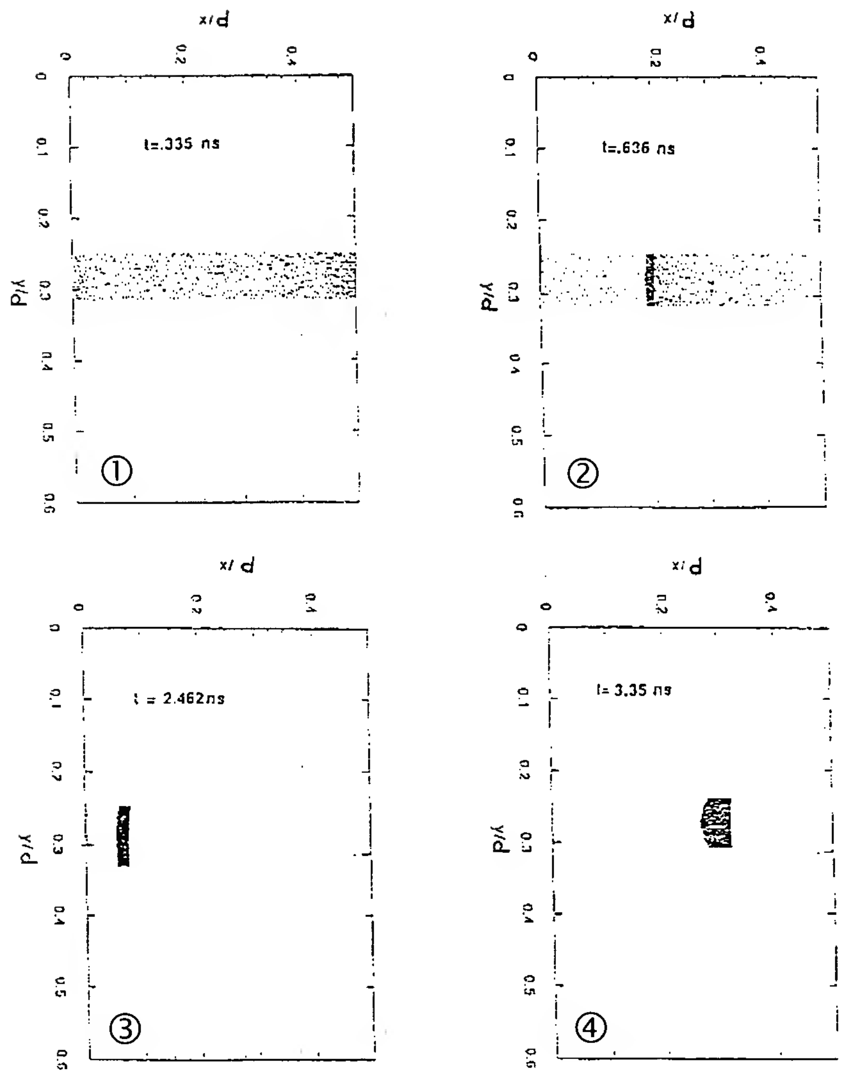

① Plot of electron distribution in the cavity at t = 0.335 ns.
② Plot of electron distribution in the cavity at t = 0.636 ns.
③ Plot of electron distribution in the cavity at t = 2.462 ns.
④ Plot of electron distribution in the cavity at t = 3.35 ns.

Figure 8: Series of time "snapshots" for a 1.3 GHz, $d = 0.5$ cm cavity using the two-dimensional PIC code with secondary emission. Note the rapid particle build-up and bunching by phase selection. Electrons traverse the horizontal axis. On the vertical axis, emission is limited to the region 0.25 to 0.32 cm.

REPLACEMENT SHEET

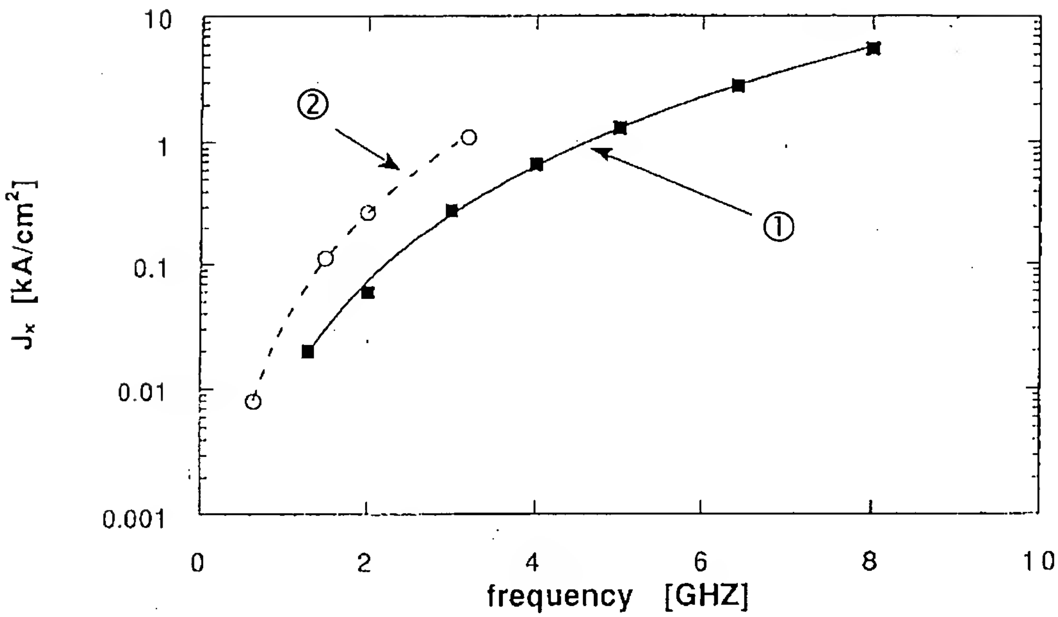

Figure 12: Steady-state current density vs. rf frequency for cavity with $\alpha_0 = 0.453$ and gap lengths of ① 0.5 cm (solid line is a fit using $J_x = 0.008f^{3.15}$) and ② 1.0 cm (dashed line is a fit using $J_x = 0.03f^{3.1}$).

REPLACEMENT SHEET

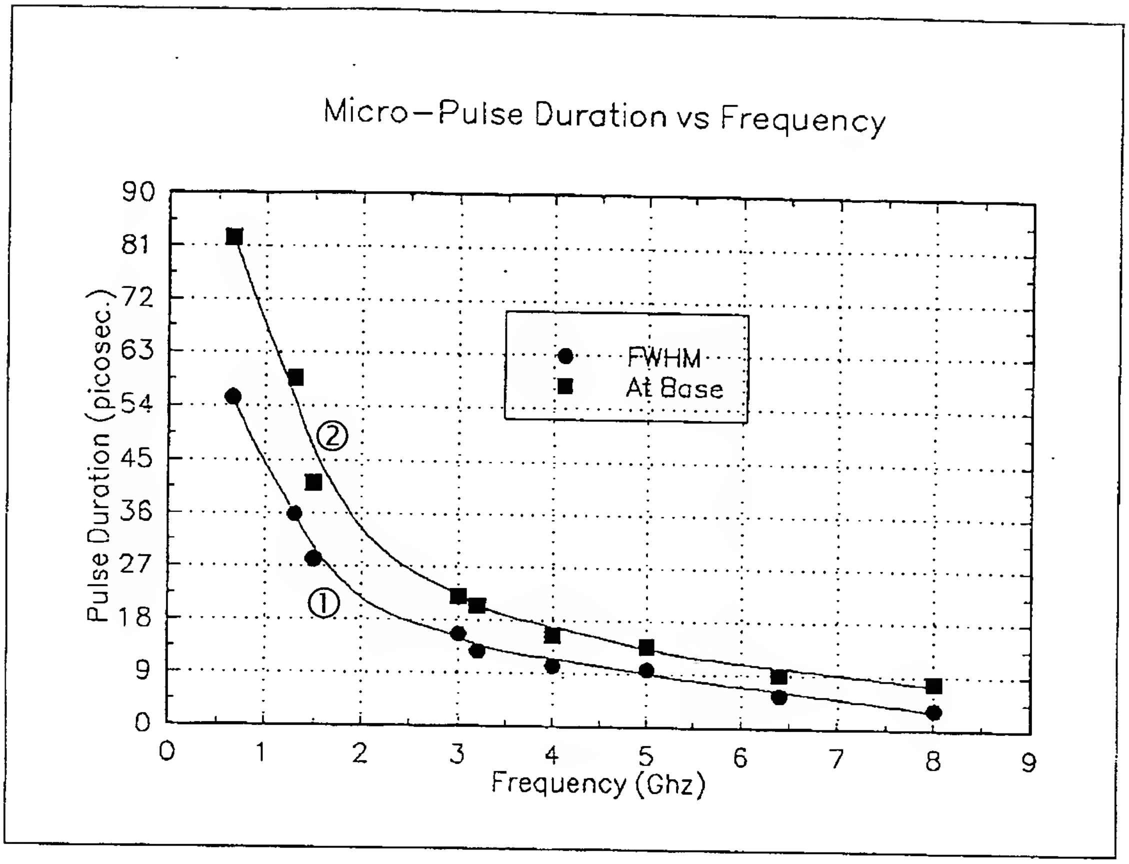

① Electron micro-pulse full width at half maximum.

② Electron micro-pulse full width at the base of the pulse.

Figure 13: Micro-pulse duration vs. frequency for $\alpha_0 = 0.453$.

REPLACEMENT SHEET

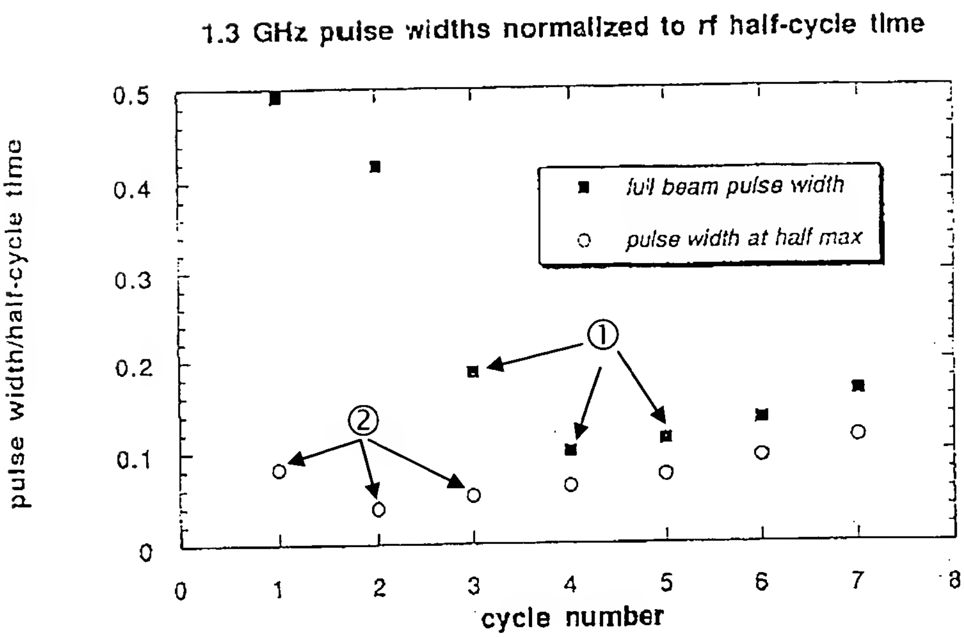

① (solid square) Beam full width at different rf cycle.

② (open circle) Beam full width at half maximum at different rf cycle.

Figure 14: Micro-pulse width (as a fraction of the half-cycle) vs. rf cycle number near the output grid. The full beam pulse width decreases with time, and reaches a minimum at the fourth rf cycle. After saturation there is a slight increase in pulse-width due to space-charge effects.

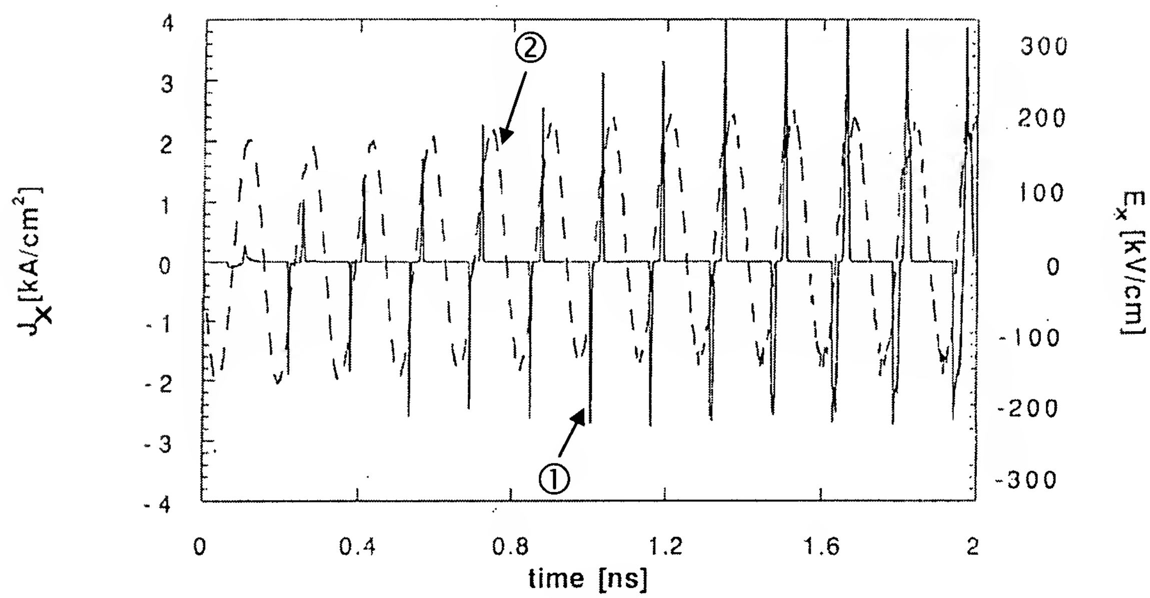

Figure 16: ① Plot of the current density in kA/cm^2 (solid line) and ② the longitudinal electric field (dashed line) for the 6.4 GHz, 105 kV simulation.

REPLACEMENT SHEET

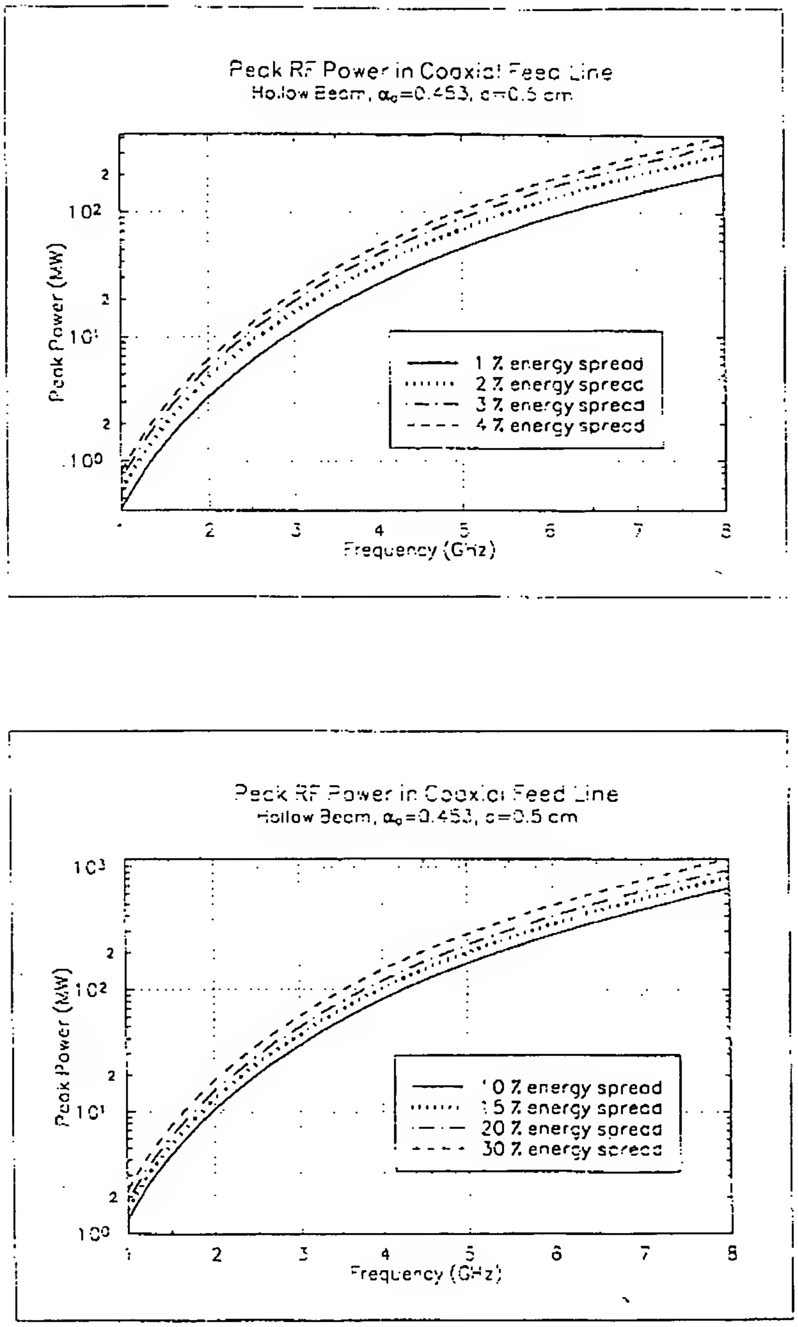

Figure 43: Peak rf power in coaxial feed line for a hollow beam, $d = 0.5$ cm.

REPLACEMENT SHEET

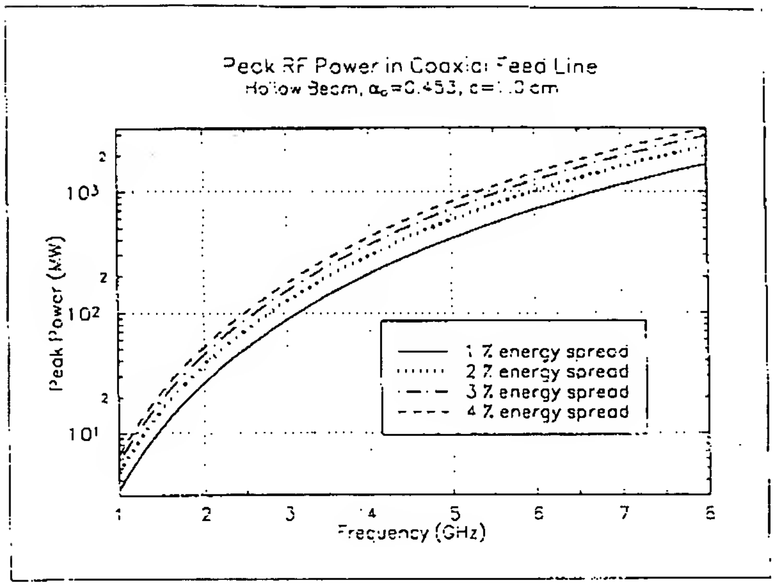

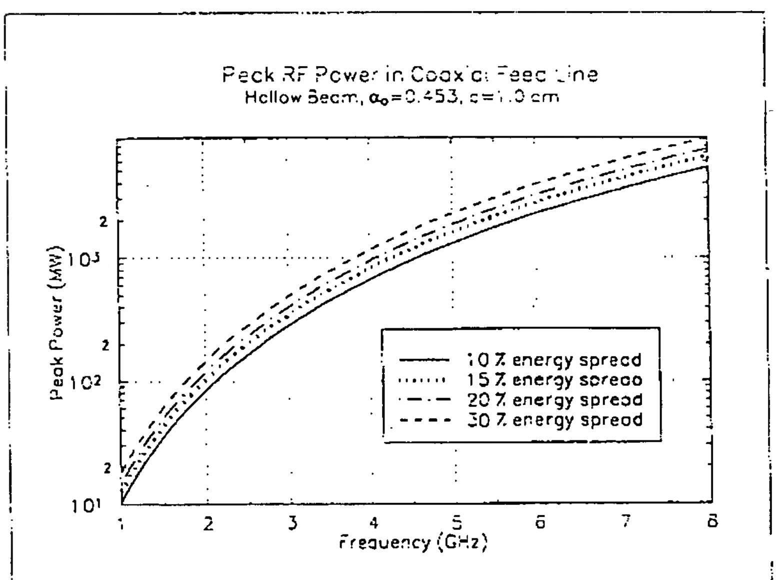

Figure 44: Peak rf power in coaxial feed line for a hollow beam, d = 1.0 cm.

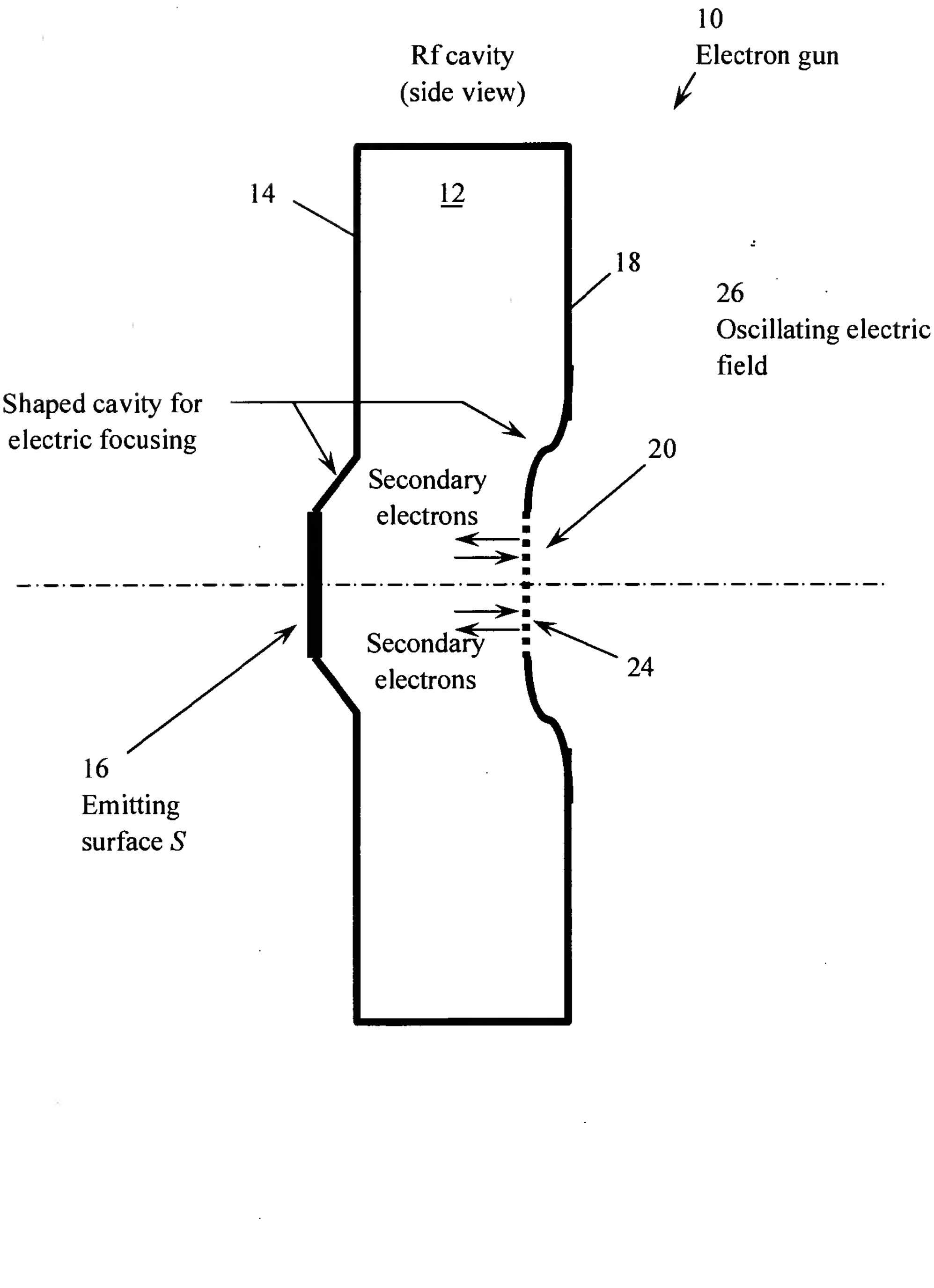

Figure 46: Schematic drawing of a possible design for electrostatic focusing in the MPG.